RSC Advances

PAPER

View Article Online
View Journal | View Issue



Cite this: *RSC Adv.*, 2020, **10**, 15139

# Fabrication of new conductive surface-metallized UHMWPE fabric with improved thermal resistance†

Qianhong Gao,[a] Minglei Wang,[bc] Jing Chen,[e] Maojiang Zhang,[bd] Jianchang Zhao,[b] Mingxing Zhang,[bc] Jiangtao Hu *[b] and Guozhong Wu *[bd]

Received 10th March 2020
Accepted 3rd April 2020

DOI: 10.1039/d0ra02228d

rsc.li/rsc-advances

A new UHMWPE-based conductive fabric was successfully prepared by radiation-induced graft polymerization and subsequent post-modification, followed by electroless deposition. The chemical structure and composition of modified UHMWPE fabrics were investigated in detail by ATR-FTIR, $^{29}$Si NMR, and XPS to confirm grafting and post-modification. After electroless deposition, the morphology, thermal stability, and crystal structure of original and modified fabrics were characterized by SEM, TG, DSC and XRD. Cu-deposited UHMWPE fabric exhibited much better thermal resistance than that of UHMWPE and Cu@UHMWPE-*g*-PAAc. In order to improve the oxidation resistance of copper-deposited fabric, nickel was processed on copper-coated UHMWPE fabric to protect the copper layer. An electromagnetic shielding effect test showed the nickel–copper coated UHMWPE fabric could shield 94.5% of the electromagnetic wave in the frequency range of 8–12 GHz. This work provides an approach for addressing the issue of poor thermal resistance of metal-coated polymeric materials due to the inherent low melting point of the organic support.



## 1. Introduction

In recent years, various fabric-based electronic products have been extensively researched and applied to next-generation wearable devices.[1] In order to combine the flexibility and comfort of the garment with the functionality of the intelligent electronic device, the fabrication of conductive flexible fabric is essential. These flexible conductive fabrics can interconnect both functional components and power, as well as the necessary substrates for the preparation of electronic components on flexible conductive fabrics.

There are mainly two general approaches that can be used to fabricate conductive fabrics.[2] Although conductive fabrics can be prepared through incorporating several conductive filler materials involving carbon nanofibers,[3] graphene sheets,[4] and conductive polymers[5,6] in the past decades, they are uneconomical and difficult to be prepared on a large scale; more importantly, the above-prepared samples exhibit high resistance. A more economical and effective method of preparing conductive textiles is to coat conventional surface with a layer of conductive materials. Metal is still the best choice in terms of cost, conductivity, and stability so far. Thus, surface metallization is still an effective strategy to fabricate conductive fabrics, which not only retains the specific properties of textiles, such as light weight, flexibility, and low cost of manufacturing, but also shows characteristics peculiar to metals.

Compared with other surface metallization methods, such as sputtering, electric plating, physical vapor deposition, and chemical vapor deposition, electroless deposition (ELD) has become a versatile and cost-efficient approach to construct high quality metal coatings, which can form metal particles on surfaces in the presence of catalysts, usually surface-immobilized metal cations, *via* an autocatalytic redox reaction.[7] In addition, this process does not require high temperature processing, expensive equipment or conductive substrates, which is very suitable for polymer substrates with low thermal resistance. Recently, a strategy for catalyst immobilization by surface-grafted polymers has attracted increasing interest due to its ability to construct polymer-bridged metal/substrate hierarchical structure *via* ELD. Therefore, several surface grafting technologies have been employed to graft polymers on various polymeric substrates for ELD, such as surface-initiated atom transfer polymerization, solution polymerization, UV-, and plasma-induced graft polymerization.[8] Since the grafted polymer chains not only can improve the adsorption efficiency and selectivity of the catalyst, but also enhance the interfacial

[a]*School of Environmental and Biological Engineering, Nanjing University of Science & Technology, 200 Xiaolingwei, Nanjing 210094, Jiangsu Province, China*

[b]*CAS Center for Excellence on TMSR Energy System, Shanghai Institute of Applied Physics, Chinese Academy of Sciences, P.O. Box 800-204, 2019 Jialuo Road, Jiading District, Shanghai 201800, China. E-mail: hujiangtao@sinap.ac.cn; wuguozhong@sinap.ac.c; Fax: +86-21-39195118; Tel: +86-21-39194531*

[c]*University of Chinese Academy of Sciences, Beijing 100049, China*

[d]*School of Physical Science and Technology, Shanghai Tech University, Shanghai 200031, China*

[e]*Anhui Institute of Product Quality Supervision and Inspection, Hefei 230051, China*

† Electronic supplementary information (ESI) available. See DOI: 10.1039/d0ra02228d

bonding strength between the substrate and the metal coating. Furthermore, it also can prevent the catalyst from falling off and causing instability of the plating solution. However, due to different shapes and chemical compositions of various polymer substrates, the above-mentioned surface treatment technologies still face many problems in actual industrial production, which may be due to complicated production processes or technically unfavorable treatment processes, resulting in difficulty in mass production. Compared with these processes, radiation-induced graft polymerization (RIGP) is favorable due to its strong penetration into the polymer trunk, uniform formation of active sites for initiating grafting, great ability to endow new performance characteristics to a material, and a clean technique in which no additional chemicals such as initiators are required.[9] Therefore, the radiation-induced graft technique is a suitable methodology for activating the surface of polymer and building a coating which is covalently grafted to the substrate and able to coordinate catalyst for the growth of the metallic phase starting inside the host polymer.[10]

Ultra-high molecular weight polyethylene (UHMWPE) fiber, a third-generation high-performance fiber, plays an important role in different industries due to its low specific weight, high wear resistance, high strength, low friction, excellent toughness, ease of manufacture, biocompatibility and biostability,[11] which can be considered as a kind of ideal candidates for preparing conductive fiber. However, to date, owing to lack of polar functional groups, low surface free energy, and smooth surface of UHMWPE fiber, only a limited number of papers about conductive fiber/fabric based on UHMWPE fiber have been reported.[12–14] Therefore, how to effectively activate the UHMWPE surface with controllable conductivity and high durability remains a challenge. In our previous work, we have successfully resolved the above problem and prepared high-performance UHMWPE-based conductive fiber through RIGP.[10] However, UHMWPE fiber is a typical flexible material with low melting point and poor thermal resistance,[15] which may result in the thermal deformation of the organic support when encountering current overload or working for a long time. More importantly, the deformation caused by heat will affect the signal stability and sensitivity when metal-coated UHMWPE fiber used as wires or sensors component in smart clothing. Thus, it is necessary to improve the thermal resistance of UHMWPE fiber.

Owing to the high thermal stability, polysiloxanes have been used to improve the thermal resistance of polymers in recent years.[16] We have reported the work on improving thermal and UV resistances of UHMWPE fabric through RIGP and *in situ* growth of organic–inorganic hybrid layers.[17] Based on the results reported in our previous works, we found that γ-methacryloxypropyl trimethoxysilane (MAPS) is liable to graft polymerization on different polymer surfaces[18–20] and can form a cross-linked Si–O–Si structure on the surface of the substrate *via* hydrolysis–condensation reaction to improve the thermal resistance; moreover, the flexibility of Si–O–Si bond is better than that of C–C bond which can effectively decrease the influence of deformation on the dimensional stability and sensitivity especially used as a wire or component for strain sensor. In addition, the grafted PMAPS chains also can be cohydrolyzed with other silane coupling agents to introduce reactive functional groups, such as mercapto, amino, epoxy, and nitrile groups and subsequently introduce different function onto the surface of organic supports.[21]

Based on the aforementioned discussion, a novel UHMWPE-based conductive fabric was fabricated through surface-grafted polymer-assisted electroless deposition. In this study, PMAPS graft chains were grafted onto the surface of UHMWPE fabric *via* RIGP technique and subsequent cohydrolyzed with *N*-(2-aminoethyl)-3-aminopropyltriethoxysilane (NAPTES), which can form an organic–inorganic hybrid coating on the surface of UHMWPE fabric and simultaneously introduce amino groups for coordinating catalyst ions. Palladium ions adsorbed by amine on the surface of UHMWPE fabric have been demonstrated to be an effective seeding and adhesion layer for subsequent ELD of copper to yield conductive textiles in which the metal-deposited textiles show excellent electrical properties and remain intact morphology. Importantly, the cross-linked organic–inorganic hybrid layer can effectively improve the thermal resistance of UHMWPE fabric.

## 2. Experimental

### 2.1 Materials

UHMWPE fabric (100%), with a surface density of 176 g $m^{-2}$ and plain weave, was purchased from Beijing Tongyizhong Special Fiber Technology Development Co., Ltd. Dimethylaminoborane (>99%) was purchased from Tokyo Chemical Industry Co. Ltd. Nickel sulfate heptahydrate (AR) was purchased from Shanghai Macklin Biochemical Co. Ltd. Palladium standard solution (1000 mg $L^{-1}$) was purchased from Guobiao (Beijing) Testing & Certification Co. Ltd. Other reagents, purchased from Sinopharm Chemical Reagent Company, were of analytical grade. All reagents were used without further purification. Deionized water was produced using a water purification system (ELGA PURELAB Classic UV).

### 2.2 Preparation of metal-coated UHMWPE fabrics

The fabrication process of copper-coated UHMWPE fabrics was illustrated in detail in Scheme 1. The UHMWPE fabrics grafted with MAPS were prepared according to the procedures reported earlier by our group.[17] The degree of grafting (Dg) of the grafted UHMWPE fabric was determined according to the following equation:

$$\mathrm{Dg}\ (\%) = (W_1 - W_0)/W_0 \times 100 \quad (1)$$

where $W_0$ and $W_1$ are the weights of the samples before and after grafting polymerization, respectively. In present study, the Dg of UHMWPE-*g*-PMAPS was 36.5%. Appropriate quantities of UHMWPE-*g*-PMAPS, deionized water, ethanol, NAPTES, and ammonia (0.2 wt%) were put into a three-necked flask equipped with a thermometer and condenser. The mixture was maintained at 25 °C with stirring for 48 h. After that, the resultant was removed from the three-necked flask and repeatedly washed 3 times with water and 3 times with ethanol,

 

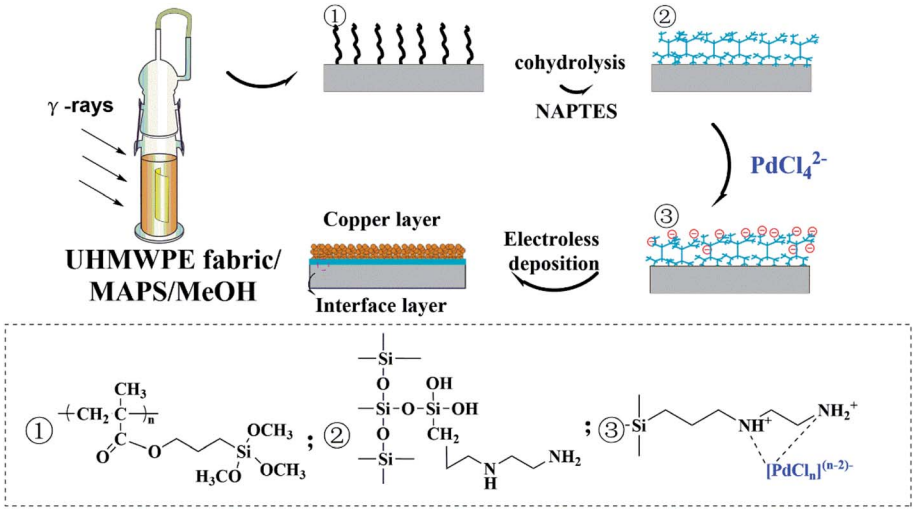


Scheme 1 Schematic illustration of the process of preparing conductive UHMWPE fabrics.

subsequently vacuumly dried at 60 °C. The resultant was denoted as UHMWPE-*g*-PMAPS-NAPTES.

Surface Activation Step: The grafted UHMWPE fabrics were first activated through the immobilization of the Pd catalyst for the subsequent electroless deposition of Cu. In detail, UHMWPE-*g*-PMAPS-NAPTES were immersed into palladium chloride solution (50 mg $L^{-1}$) for 5 min at room temperature to induce an ion-adsorption process. Afterward, samples were rinsed several times with deionized water.

Metallization step: two plating baths were tested. The first one consist of 6 g $L^{-1}$ $CuSO_4 \cdot 5H_2O$, 15 g $L^{-1}$ $Na_3C_6H_5O_7 \cdot 2H_2O$, 28 g $L^{-1}$ $NaH_2PO_3$, 30 g $L^{-1}$ $H_3BO_3$, 0.5 g $L^{-1}$ $NiSO_4 \cdot 7H_2O$. The surface-activated UHMWPE-*g*-PMAPS-NAPTES were placed in the above-mentioned plating baths for different time to electroless deposition of copper. The reaction was carried out at 65 °C with a pH value of 9.2 and the solid–liquid ratio was 5 g $L^{-1}$. After that, the copper-coated UHMWPE fabrics (abbreviated as Cu@UHMWPE-*g*-PMAPS-NAPTES) were washed in deionized water and then dried in a vacuum oven at 60 °C for 24 h. For the second case, a homemade electroless nickel plating bath was used which contained 25 g $L^{-1}$ $NiSO_4 \cdot 7H_2O$ as a source of $Ni^{2+}$ ions, 1.5 g $L^{-1}$ $C_2H_{10}BN$, 50 g $L^{-1}$ $Na_4P_2O_7 \cdot 10H_2O$, 45 mL $L^{-1}$ ammonia with a pH value of 10.7. The obtained copper-coated UHMWPE fabrics is immersed into the above plating solution for 15 minutes to deposit nickel layer, which can improve the oxidation resistance of copper coating.

### 2.3 Characterization

The chemical structure of the UHMWPE fabrics was determined by a Bruker Tensor 207 Fourier transform infrared spectrometry (FTIR) by the accumulation of 32 scans with a resolution of wave number 4 $cm^{-1}$ in the attenuated total reflection (ATR) mode. The chemical composition of UHMWPE fabrics was investigated *via* a Kratos Axis-Ultra DLD X-ray photoelectron spectroscopy (XPS) using monochromatic Al Kα radiation under the chamber pressure of $10^{-9}$ Torr from a 250 W X-ray source. $^{29}Si$ solid-state nuclear magnetic resonance ($^{29}Si$ NMR) spectrum of UHMWPE-*g*-PMAPS and UHMWPE-*g*-PMAPS-NAPTES were tested by a Bruker 400 MHz NMR spectrometer. In order to observe the surface morphology and microstructure of the UHMWPE fabrics, all the tested samples were coated with a thin gold layer and a ZEISS GeminiSEM 300 scanning electron microscope (SEM). Electrical conductivity of the metal-coated UHMWPE fabrics was measured by a surface high-impedance analyzer McP-HT450 and a surface low-impedance analyzer Mcp-HT610 from Mitsubishi Corporation. Thermogravimetric analysis (TGA) was performed on a NETZSCH TG 209 F3 instrument to assess the thermal stability of the modified cotton fabrics. The specimens were heated from 50 to 700 °C at a heating rate of 10 °C $min^{-1}$ under nitrogen atmosphere. Differential scanning calorimetry (DSC) were carried out by using a PerkinElmer DSC-822e analyzer. The measurements were performed from 40 to 180 °C with a heating rate of 10 °C $min^{-1}$ in a nitrogen atmosphere with a gas flow of 20 mL $min^{-1}$. Wide angle X-ray diffraction (WAXD) curves were measured on a Bruker D8 Advance diffractometer with a Bragg–Brentano geometry using Cu-Kα radiation ($\lambda = 1.5418$ Å) at an operating voltage of 40 kV. The electromagnetic shielding effect of copper (nickel) coated UHMWPE fabrics was evaluated by a coaxial network method using Agilent N5242A vector network analyzer with a test frequency range of 8.0 to 12.0 GHz.

## 3. Result and discussion

### 3.1 Graft polymerization

The effect of monomer concentration in methanol on the grafting process has been investigated and shown in Fig. 1. It is clear that the Dg increases with the increase of the monomer concentration due to the high concentration of monomers available to react with the free radical formed in the polymer backbone. From above results, it can be concluded that the Dg is directly proportional to the monomer concentration. Thus, it allows for a selection of suitable monomer concentration to

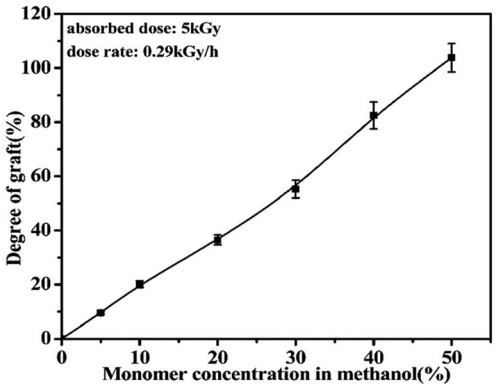


Fig. 1 Effect of monomer concentrations on the degree of grafting.

obtain a reasonable grafting degree which possessed excellent comprehensive performance for the subsequent ELD process.

### 3.2 Characterization

Fig. 2A exhibits the ATR-FTIR spectra of the original and modified fabrics. Compared with the pristine UHMWPE fabric, UHMWPE-*g*-PMAPS presented several new absorption bands at 1726,1260,1190,1080, and 820 $cm^{-1}$, which were attributed to the stretching vibrations of –C=O, –O–C, –Si–O–Me, and Si–C, respectively.[22] After cohydrolysis with NAPTES, there are new characteristic peaks belonging to Si–O–Si groups in the range of 1000–1110 $cm^{-1}$, suggesting that Si–O–Me groups were changed into siloxane.[23] While a small peak centered at 917 $cm^{-1}$ representing Si–OH groups also can be observed, demonstrating that some Si–O–Me groups were hydrolyzed to form Si–OH. An additional peak centered at 1560 $cm^{-1}$ corresponding to –N–H in NAPTES is observed,[24] indicating that the immobilization of NAPTES molecular chains on the surface of UHMWPE-*g*-PMAPS *via* the sol–gel reaction between PMAPS and NAPTES. The presence of the –N–H group provides adsorption sites for the adsorption of palladium ions for subsequent ELD process.

Varieties in surface chemical composition were also confirmed by the results of the X-ray photoelectron spectroscopy (XPS) and shown in Fig. 2B. Compared to the spectrum of original UHMWPE fabric, UHMWPE-*g*-PMAPS displayed the peaks of Si2s (152.6 eV) and Si2p (102.1 eV), suggesting that PMAPS graft chains existed on the surface of UHMWPE fabric. With regard to the spectrum of UHMWPE-*g*-PMAPS-NAPTES fabric, an additional characteristic peak of N1s was found at 398.3 eV. Meanwhile, the intensity of characteristic peaks of Si2s and Si2p increased after the coating of NAPTES *via* sol–gel reaction. The XPS spectra confirmed that the organic–inorganic hybrid structure formed through the co-hydrolysis of PMAPS and NAPTES were successfully coated on the surface of UHMWPE fabric bridged by a covalent bond.

Fig. 2C and D illustrate the solid-state $^{29}Si$ NMR spectra of UHMWPE-*g*-PMAPS and UHMWPE-*g*-PMAPS-NAPTES at 20 °C. It could be seen that UHMWPE-*g*-PMAPS displayed a well-

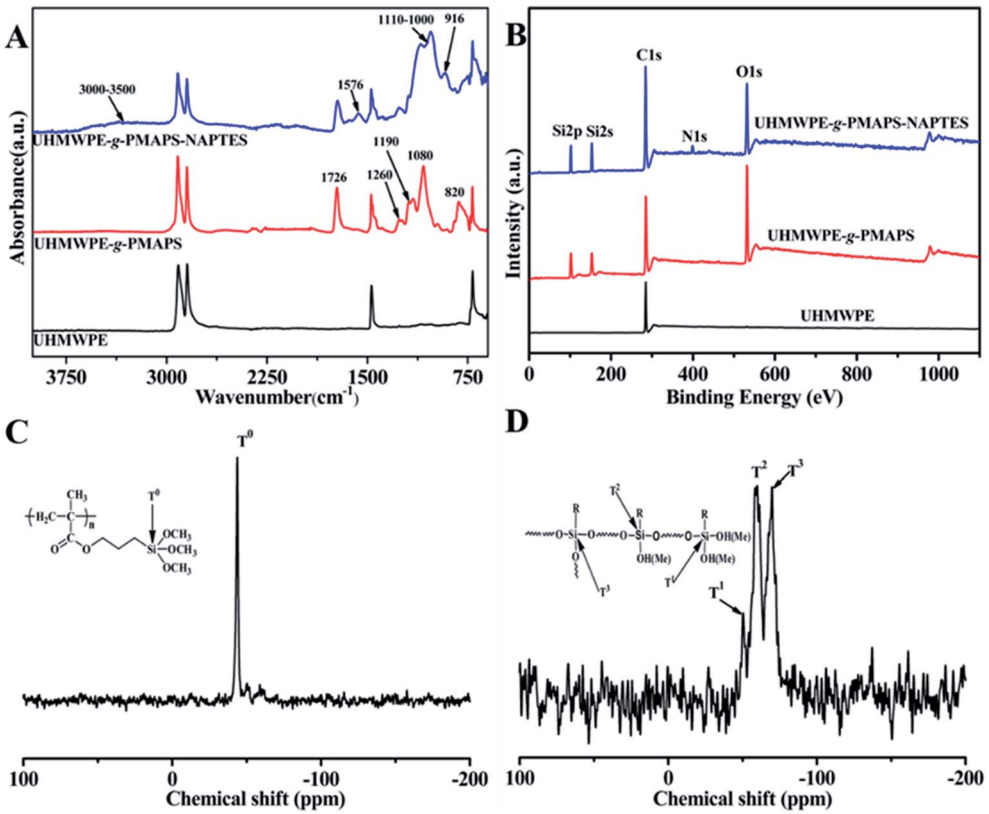


Fig. 2 ATR-FTIR (A) and XPS (B) spectra of the pristine UHMWPE, UHMWPE-*g*-PMAPS and UHMWPE-*g*-PMAPS-NAPTES fabrics; the solid-state $^{29}Si$ NMR spectra of UHMWPE-*g*-PMAPS (C) and UHMWPE-*g*-PMAPS-NAPTES (D).

 

defined singlet at −43.8 ppm corresponding to $T^0$, which was the characteristic resonance of the silicon nucleus for PMAPS ($-CH_2CH_2-Si(OCH_3)_3$).[18] In addition, the presence of a single peak also suggested that the graft chains did not undergo hydrolysis with the moisture in air during the grafting process. After the reaction of cohydrolysis with NAPTES, the spectrum of UHMWPE-*g*-PMAPS-NAPTES showed three signals at −50.3, −59.8, and −69.8 ppm, which can be assigned to silicon species of T1($-CH_2CH_2-Si(OSi)(OR)_2$), T2($-CH_2CH_2-Si(OSi)_2(OR)$), and $T^3$($-CH_2CH_2-Si(OSi)_3$),[25–27] respectively. This suggested that after the cohydrolysis of PMAPS and NAPTES, the surface of the obtained UHMWPE-*g*-PMAPS-NAPTES was covered by a novel hyperbranched polysiloxane consisting of linear networks, dimeric structures, and three-dimensional branched architectures. In all, the above results demonstrate that MAPS monomer is successfully grafted on UHMWPE fabric by RIGP and the post-modification with NAPTES is effectively completed.

### 3.3 Electroless deposition

Palladium is acted as an effective catalyst for ELD of Cu and other metals. In order to decrease the diffusion of catalyst into plating solution, UHMWPE-*g*-PMAPS-NAPTES-Pd was rinsed with deionized water. The UHMWPE-*g*-PMAPS-NAPTES fabric was finally coated with a layer of Cu particles by immersing in a homemade ELD bath. After the ELD process triggered by Pd, the deposited metal will initiate the autocatalytic metallization process. Effect of electroless deposition time on the weight increase was plotted, as illustrated in Fig. 3A. In the first 90 min of ELD, it can be seen that the weight increased as a linear function of ELD time. The weight gain reached 29.4% of its original weight after 120 min, and then almost level off because of the decrease of $Cu^{2+}$ ion concentration in ELD bath.

The sheet resistance of the Cu@UHMWPE-*g*-PMAPS-NAPTES was also measured *via* a four-probe measurement, which is a standard method for measuring the resistance of thin film. The average sheet resistance of Cu@UHMWPE-*g*-PMAPS-NAPTES against the ELD time was plotted and shown in Fig. 3B. The UHMWPE-*g*-PMAPS-NAPTES was electrically insulated. After 20 minutes of ELD, though the sample became electrically conductive, its sheet resistance was up to 125.6 Ω $sq^{-1}$ and exhibited poor conductivity. In addition, most of the surface of the Cu@UHMWPE-*g*-PMAPS-NAPTES still remained black, which may be ascribed to the color of Pd particles. Before the deposition of metal copper on the surface of the fabric, palladium ions were first reduced by sodium hypophosphite in the bath, and then Pd atoms act as a catalyst for subsequent metal deposition. The Pd particles did not have enough time to catalyze the reduction of copper ions and were still adsorbed on the surface of the sample. So, it is mainly the reduction process of palladium ions in the first 20 minutes. The resistance of Cu@UHMWPE-*g*-PMAPS-NAPTES gradually decreased with the prolongation of plating time. When the ELD time was extended to 120 minutes, black areas almost disappeared and the surface of the Cu@UHMWPE-*g*-PMAPS-NAPTES exhibited a red copper color, and the sheet resistance decreased to 1.65 Ω $sq^{-1}$. Further extend the plating time, the sheet resistance showed a little decrease (0.05 Ω $sq^{-1}$) and then remained almost constant even for the deposition time longer than 240 minutes, which was consistent with the weight gain. Considering all factors including efficiency, cost, and conductivity, 120 minutes of the ELD is suitable for copper deposition.

### 3.4 Surface morphological structure

The effects of surface modification on materials will also be reflected in the morphologies of fibers. Fig. 4 shows SEM images of UHMWPE, UHMWPE-*g*-PMAPS, and Cu deposited UHMWPE fabrics. The pristine UHMWPE fiber has smooth and clean surface, and there are some narrow and shallow grooves along the axial direction, indicating that the molecular chains arrange in the longitudinal direction. After graft polymerization, UHMWPE-*g*-PMAPS exhibits uneven surfaces and obvious protrusions caused by the accumulation of grafting chains (Fig. 4B and B′). With regard to Cu@UHMWPE-*g*-PMAPS-NAPTES, after the ELD process, the surface is covered by a layer of uniformly distributed and densely packed copper particles (Fig. 4C and C′). The formed copper film continuously and uniformly surrounds every fiber, and no obvious pores caused by the hydrogen evolution can be detected.

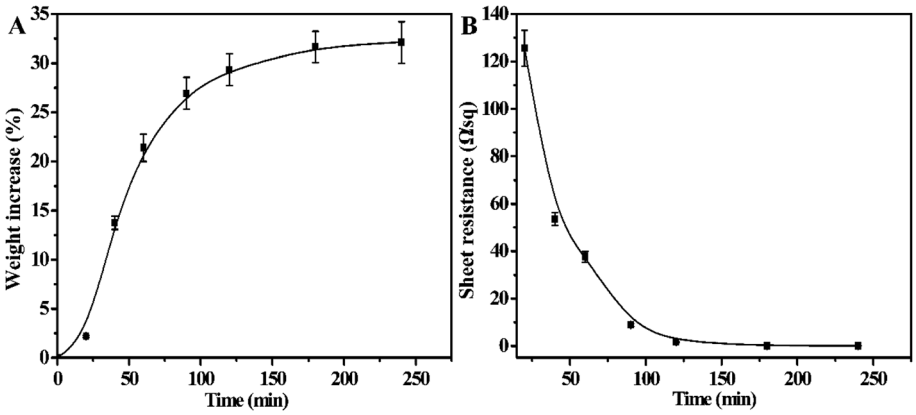


Fig. 3 Weight increase (A) and sheet resistance (B) of UHMWPE fabric at different plating times.

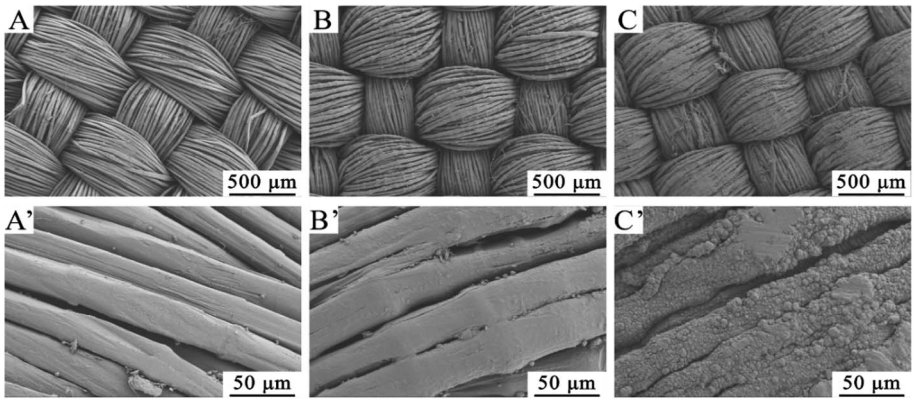


Fig. 4 Scanning electron micrographs of UHMWPE fabric, UHMWPE-*g*-PMAPS, and Cu@UHMWPE-*g*-PMAPS-NAPTES (A, B, C×100; A′, B′, C′ × 5000).

### 3.5 Thermal properties

Fig. 5 shows the TG and DTG curves of original and modified fabrics, the corresponding parameters such as the initial decomposition temperature ($T_{di}$), the temperature of the maximum degradation rate ($T_{max}$), and the char yield ($Y_c$) at 700 °C are summarized in Table 1. The samples exhibit different $T_{di}$, $T_{max}$, and $Y_c$ values, indicating that surface modification changed the thermal degradation mechanisms as compared to the pristine UHMWPE fabric. The decrease of $T_{di}$ of treated fabrics likely ascribes to the low molecular weight and poor heat stability of the graft chains. After the cohydrolysis of PMAPS graft chains with NAPTES, the thermal stability was improved because of the formation of cross-linked three-dimensional network structure of siloxane. Note that the typical parameters of Cu@UHMWPE-*g*-PMAPS-NAPTES, expect $T_{max}$, are slightly better than those of UHMWPE-*g*-PMAPS-NAPTES. This is attributed to the fact that metal copper has excellent thermal stability compared with that of organic–inorganic hybrid coating and UHMWPE fiber matrix; furthermore, the deposition of copper particles means the formation of a dense layer which, to some extent, is conducive to isolate the fabric from air and then prevent the combustion of the fabrics. After the deposition of copper nanoparticles, the value of $T_{max}$ decreased as compared with other samples. The cause behind this phenomenon may be due to the catalytic degradation of copper nanoparticles which decrease the heat resistance of the material.

The pristine UHMWPE and copper-coated UHMWPE fabrics were subjected to differential scanning calorimetry (DSC). The DSC curves are presented in Fig. 6. The control UHMWPE fabric exhibited two endotherms, that is a main peak at 148.3 °C and a shoulder peak at 156.2 °C, which was consistent with the phenomenon reported in previous literatures.[28,29] From the spectrum of Cu@UHMWPE-*g*-PMAPS-NAPTES, it can be seen that the $T_m$ (melting temperature) of Cu@UHMWPE-*g*-PMAPS-NAPTES reached 158.7 °C, which increased by 10 °C as compared with that of the pristine UHMWPE fabric. For comparison, the DSC curve of Cu@UHMWPE-*g*-PAAc was also provided. For the fairness of comparison, UHMWPE-*g*-PAAc (abbreviation for acrylic acid grafted on UHMWPE) with a similar Dg and deposited amount of copper was employed. Under the same conditions, Cu@UHMWPE-*g*-PAAc exhibits a lower $T_m$ as compared with Cu@UHMWPE-*g*-PMAPS-NAPTES, demonstrating that the formation of the organic-inorganic hybrid networks from the cohydrolysis between PMAPS and NAPTES can effectively restrict UHMWPE chain relaxation near the defect–crystal interfaces.

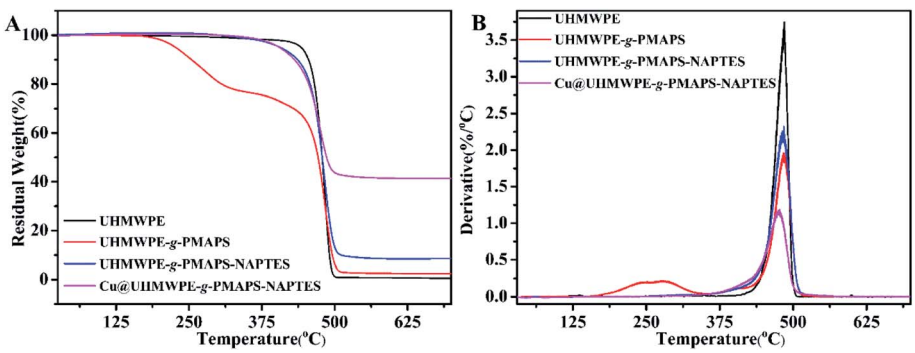


Fig. 5 TG and DTG curves of pristine UHMWPE, UHMWPE-*g*-PMAPS, UHMWPE-*g*-PMAPS-NAPTES and Cu@UHMWPE-*g*-PMAPS-NAPTES fabrics in $N_2$ atmosphere.

 

Table 1 Characteristic data from TG analyses of pristine UHMWPE (A), UHMWPE-*g*-PMAPS (B), UHMWPE-*g*-PMAPS-NAPTES (C) and Cu@UHMWPE-g-PMAPS-NAPTES (D) fabrics

| Sample | $T_{di}$ (°C) | $T_{max}$ (°C) | Intensity | $Y_{c\ at\ 700\ °C}$ (%) |
|---|---|---|---|---|
| A | 442.3 | 485.2 | 3.75 | 0.60 |
| B | 227.2 | 279.4/483.9 | 0.22/1.95 | 2.4 |
| C | 405.7 | 483.9 | 2.24 | 8.5 |
| D | 405.3 | 480.3 | 1.15 | 41.4 |

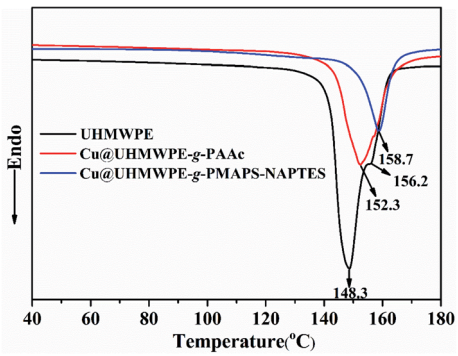


Fig. 6 DSC curves of UHMWPE, Cu@UHMWPE-*g*-PAAc and Cu@UHMWPE-*g*-PMAPS-NAPTES fabrics.

In order to verify the effectiveness of thermal resistance for the above-mentioned copper-coated UHMWPE fiber under practical condition, an electronic circuit was constructed through linking a 9 V battery and one electrical contact of a lamp *via* the as-made conductive UHMWPE fibers (Fig. 7). When the lamp and the battery were contacted with Cu@UHMWPE-*g*-PAAc fiber, the conductive fiber was severely deformed due to the thermal effect of the current, making it difficult to provide a stable power for the lamp, as shown in Fig. 7A and Video S1.† When Cu@UHMWPE-*g*-PMAPS-NAPTES fiber was utilized as an electrical wire for powering a lamp, the lamp can be lighted up immediately and illuminated until it was disconnected (see Fig. 7B and Video S2†). More importantly, this as-prepared conductive fiber will not be thermally deformed due to current overload or working for a long time.

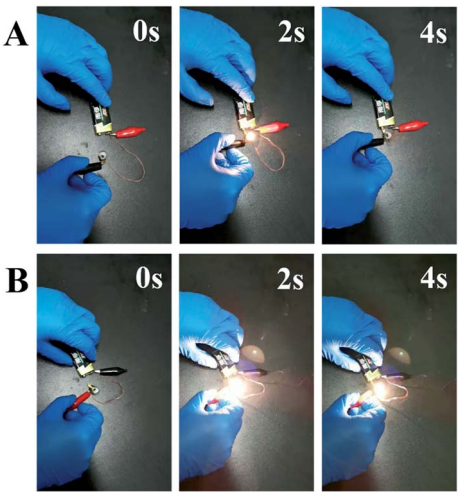


Fig. 7 Digital images of Cu@UHMWPE-*g*-PAAc fiber (A) and Cu@UHMWPE-*g*-PMAPS-NAPTES fiber (B) are used as an electrical wire for powering a lamp at different time.

### 3.6 Stability in air

The stability of the conductance is very important in practical applications because it determines the signal transmission efficiency and thermal yield of the device. So, the conductivity changes of the Cu@UHMWPE-*g*-PMAPS-NAPTES and Ni–Cu@UHMWPE-*g*-PMAPS-NAPTES under aging was evaluated and shown in Fig. 8. After 9 days of aging, the sheet resistance increased by 160% and then remained almost constant with prolonging the aging time indicating the long-term stability. Based on the previous studies, the increase in resistivity was ascribed to the partial oxidation of Cu deposited on the surface of UHMWPE fabric into copper oxide.[10,30] This instability may be solved by capping a layer of air-stable conductive metals, such as nickel. As proof-of concept, here we used nickel as protective layer to deposit on the surface of Cu-coated UHMWPE fabric because of the excellent aging resistance of nickel. After electroless copper plating, the Cu-deposited sample was dipped into the electroless plating bath of nickel for 15 min, and a layer of nickel was formed because of the autocatalytic reduction reaction. The sheet resistance of the as-made Ni–Cu@UHMWPE-*g*-PMAPS-NAPTES was electrically conductive with good air stability.

### 3.7 XRD analysis

Above results indicate that Ni–Cu@UHMWPE-*g*-PMAPS-NAPTES and the pristine UHMWPE fabric have different chemical structures, then whether irradiation, graft polymerization, and sol–gel processes can change the aggregation structure of UHMWPE fabric? To further clarify this question,

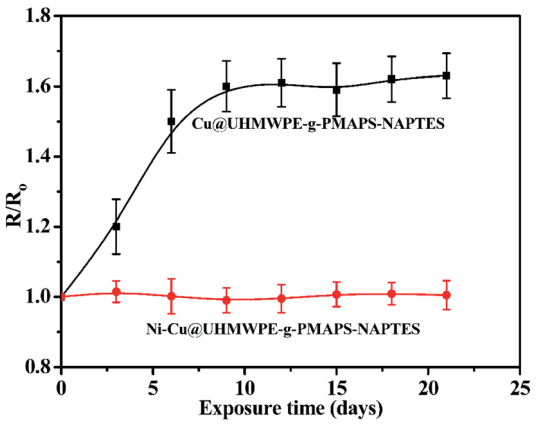


Fig. 8 Resistance aging test of Cu@UHMWPE-*g*-PMAPS-NAPTES and Ni–Cu@UHMWPE-*g*-PMAPS-NAPTES ($R$ and $R_0$ are the resistance of Cu@UHMWPE-*g*-PMAPS-NAPTES and Ni–Cu@UHMWPE-*g*-PMAPS-NAPTES before and after aging).

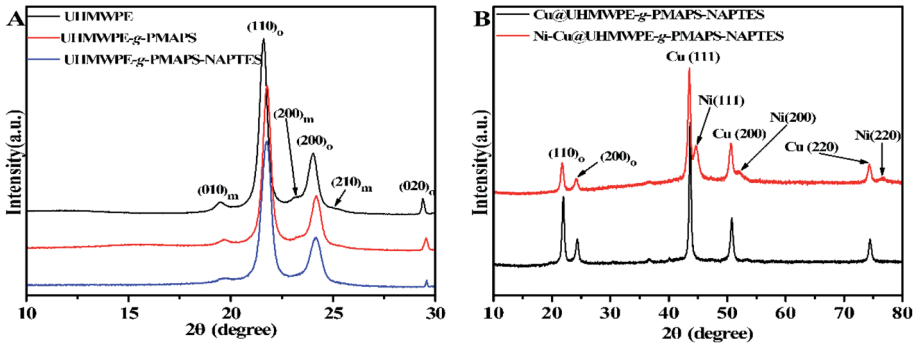


Fig. 9 XRD patterns of pristine UHMWPE, UHMWPE-*g*-PMAPS, UHMWPE-*g*-PMAPS-NAPTES, Cu@UHMWPE-*g*-PMAPS-NAPTES, and Ni–Cu@UHMWPE-*g*-PMAPS-NAPTES fabrics.

the XRD patterns of UHMWPE, UHMWPE-*g*-PMAPS, UHMWPE-*g*-NAPTES, Cu@UHMWPE-*g*-NAPTES, and Ni–Cu@UHMWPE-*g*-NAPTES fabrics were performed. As shown in Fig. 9, UHMWPE, UHMWPE-*g*-PMAPS, and UHMWPE-*g*-NAPTES have the similar XRD patterns as pristine UHMWPE fabric, each of them shows four peaks which ascribe to the (010), (110), (200), and (020) peaks within the range of 19–30°, indicating that UHMWPE, UHMWPE-*g*-PMAPS, and UHMWPE-*g*-PMAPS-NAPTES have the same crystal structure as UHMWPE fabric,[31] that is, radiation-induced graft polymerization, and sol–gel processes only changes the chemical structure, but does not change the aggregation structure of UHMWPE fabric. X-ray diffraction was also conducted to study the crystalline structures of the resultant Cu and Ni–Cu layer. Fig. 9B shows the XRD patterns of Cu and Ni–Cu patterns deposited on the surface of UHMWPE-*g*-PMAPS-NAPTES. Both samples before and after Ni deposited on the surface of Cu@UHMWPE-*g*-PMAPS-NAPTES show two characteristic peaks for crystalline metallic copper at 43.5°, 50.8°, and 74.5° for the Bragg's reflection indices of the (111), and (220) planes in the FCC structure.[2] After deposition of a thin nickel film, two minor diffraction peaks at 44.7° and 76.8°, ascribed to the crystalline metallic nickel,[32] were also found in the XRD patterns of Ni–Cu@UHMWPE-*g*-PMAPS-NAPTES, indicating the formation of air-stable protective layer on Cu@UHMWPE-*g*-PMAPS-NAPTES surface.

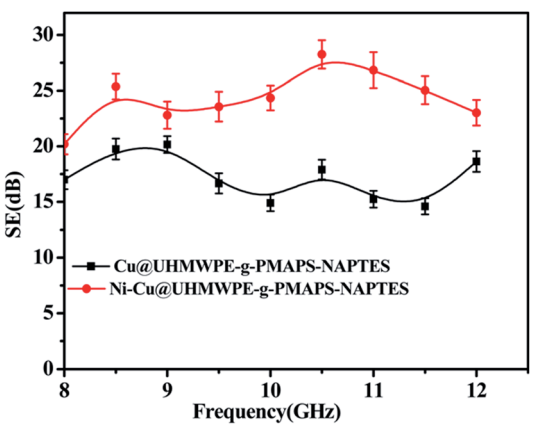


Fig. 10 Electromagnetic shielding effectiveness of Ni–Cu@UHMWPE-*g*-PMAPS-NAPTES and Cu@UHMWPE-*g*-PMAPS-NAPTES fabrics.

### 3.8 Electromagnetic shielding

With the wide application of electromagnetic radiation-emitting devices, electromagnetic shielding has aroused great concern because it not only impacts the performance of electronic devices, but also has a potential threat to human health. Shielding effectiveness (SE) of the Cu@UHMWPE-*g*-PMAPS-NAPTES and Ni–Cu@UHMWPE-*g*-PMAPS-NAPTES fabrics in the frequency range of 8.0–12.0 GHz was measured to evaluate their electromagnetic shielding ability (Fig. 10). Owing to their electrical conductivity, Cu@UHMWPE-*g*-PMAPS-NAPTES and Ni–Cu@UHMWPE-*g*-PMAPS-NAPTES fabrics can effectively reflect and absorb radiation, leading to excellent electromagnetic shielding performances. The average SE of Cu@UHMWPE-*g*-PMAPS-NAPTES and Ni–Cu@UHMWPE-*g*-PMAPS-NAPTES fabrics are ~18.5 and ~25.0 dB, respectively, which are comparable to that of commercially available SE fabrics. The *in situ* deposition of a nickel layer not only improves the shielding effectiveness of Cu@UHMWPE-*g*-PMAPS-NAPTES, but also prevents the oxidation of copper and makes electrical conductivity of Ni–Cu@UHMWPE-*g*-PMAPS-NAPTES stable, which both play a positive role to improve the effect of electromagnetic interference shielding.

## 4. Conclusion

PMAPS polymer chains were successfully grafted onto the UHMWPE fabric through simultaneous radiation-induced graft polymerization and then the cohydrolysis reaction with NAPTES, which were demonstrated by ATR-FTIR, XPS, and solid-state $^{29}$Si NMR. Then ELD of copper particles on UHMWPE-*g*-PMAPS-NAPTES fabric forms polymer-bridged copper/UHMWPE hierarchical structures, leading to the formation of conductive UHMWPE fabric. The as-made UHMWPE fabric sample showed sheet resistance as low as 0.05 Ω sq$^{-1}$, which can be utilized as a flexible electromagnetic shielding material. Moreover, due to the organic–inorganic coating on the surface of UHMWPE fabric, the thermal properties of Cu@UHMWPE-*g*-PMAPS-NAPTES were enhanced

 

relative to those of UHMWPE and Cu@UHMWPE-*g*-PAAc fabrics. In addition, this conductive UHMWPE fabric has broad application prospects in flexible electronics, radiation and electromagnetic protection and biomedical industries.

## Conflicts of interest

There are no conflicts to declare.

## Acknowledgements

We greatly appreciate supports from Science Challenge Program (No. TZ2018004), State Key Laboratory for Modification of Chemical Fibers and Polymer Materials, Donghua University, and State Key Laboratory of NBC Protection for Civilian.

## References

1 W. Zeng, L. Shu, Q. Li, S. Chen, F. Wang and X. M. Tao, *Adv. Mater.*, 2014, **26**, 5310–5336.
2 X. Q. Liu, H. X. Chang, Y. Li, W. T. S. Huck and Z. J. Zheng, *ACS Appl. Mater. Interfaces*, 2010, **2**, 529–535.
3 L. F. Zhang, A. Aboagye, A. Kelkar, C. L. Lai and H. Fong, *J. Mater. Sci.*, 2014, **49**, 463–480.
4 Y. N. Meng, Y. Zhao, C. G. Hu, H. H. Cheng, Y. Hu, Z. P. Zhang, G. Q. Shi and L. T. Qu, *Adv. Mater.*, 2013, **25**, 2326–2331.
5 Y. Y. Smolin, M. Soroush and K. K. S. Lau, *Ind. Eng. Chem. Res.*, 2017, **56**, 6221–6228.
6 A. Andreatta, C. Yong, J. C. Chiang, A. J. Heeger and P. Smith, *Synth. Met.*, 1988, **26**, 383–389.
7 S. C. Liu, M. J. Hu and J. Yang, *J. Mater. Chem. C*, 2016, **4**, 1320–1325.
8 X. Q. Liu, X. C. Zhou, Y. Li and Z. J. Zheng, *Chem.–Asian J.*, 2012, **7**, 862–870.
9 A. E. H. Ali and A. A. Aal, *Polym. Adv. Technol.*, 2009, **20**, 729–735.
10 Q. H. Gao, J. T. Hu, Y. Yang, M. L. Wang, M. J. Zhang, Z. F. Tang, M. X. Zhang, W. H. Liu and G. Z. Wu, *Ind. Eng. Chem. Res.*, 2019, **58**, 935–943.
11 S. P. Lin, J. L. Han, J. T. Yeh, F. C. Chang and K. H. Hsieh, *Eur. Polym. J.*, 2007, **43**, 996–1008.
12 W. W. Hu, Z. X. Zeng, Z. B. Wang, C. Y. Liu, X. D. Wu and Q. Gu, *J. Appl. Polym. Sci.*, 2013, **128**, 1030–1035.
13 J. H. Hong, Z. J. Pan, L. Tian, M. Yao, H. B. Wang, J. G. Chen and Y. X. Zhang, *Synth. Met.*, 2015, **209**, 512–520.
14 K. Wang, M. Q. Liu, C. Y. Song, L. Shen, P. Chen and S. A. Xu, *Mater. Des.*, 2018, **148**, 167–176.
15 Z. M. Yang, J. X. Liu, F. C. Wang, S. K. Li and X. Y. Feng, *Compos. Struct.*, 2019, **229**, 13.
16 X. B. Wang, C. Tang, Q. Wang, Y. C. Lu and X. Liu, *AIP Adv.*, 2018, **8**, 9.
17 J. T. Hu, Q. H. Gao, L. Xu, M. X. Zhang, Z. Xing, X. J. Guo, K. Zhang and G. Z. Wu, *ACS Appl. Mater. Interfaces*, 2016, **8**, 23311–23320.
18 Q. H. Gao, J. T. Hu, R. Li, L. J. Pang, Z. Xing, L. Xu, M. H. Wang, X. J. Guo and G. Z. Wu, *Carbohydr. Polym.*, 2016, **149**, 308–316.
19 M. L. Wang, M. J. Zhang, L. J. Pang, C. G. Yang, Y. M. Zhang, J. T. Hu and G. Z. Wu, *J. Colloid Interface Sci.*, 2019, **537**, 91–100.
20 J. T. Hu, Q. H. Gao, L. Xu, M. L. Wang, M. J. Zhang, K. Zhang, W. H. Liu and G. Z. Wu, *J. Mater. Chem. A*, 2018, **6**, 6085–6095.
21 S. Mallakpour and M. Madani, *Prog. Org. Coat.*, 2015, **86**, 194–207.
22 J. P. Matinlinna, S. Areva, L. V. J. Lassila and P. K. Vallittu, *Surf. Interface Anal.*, 2004, **36**, 1314–1322.
23 D. X. Zhuo, A. J. Gu, G. Z. Liang, J. T. Hu, L. Yuan and X. X. Chen, *J. Mater. Chem.*, 2011, **21**, 6584–6594.
24 W. Nowicki, A. Gasowska and P. Kirszensztejn, *Appl. Surf. Sci.*, 2016, **371**, 494–503.
25 A. G. Cunha, C. S. R. Freire, A. J. D. Silvestre, C. P. Neto and A. Gandini, *Carbohydr. Polym.*, 2010, **80**, 1048–1056.
26 L. S. Fu, R. A. S. Ferreira, N. J. O. Silva, L. D. Carlos, V. D. Bermudez and J. Rocha, *Chem. Mater.*, 2004, **16**, 1507–1516.
27 S. S. Silva, R. A. S. Ferreira, L. S. Fu, L. D. Carlos, J. F. Mano, R. L. Reis and J. Rocha, *J. Mater. Chem.*, 2005, **15**, 3952–3961.
28 Y. K. Kwon, A. Boller, M. Pyda and B. Wunderlich, *Polymer*, 2000, **41**, 6237–6249.
29 C. S. Li, M. S. Zhan, X. C. Huang and H. Zhou, *Polym. Test.*, 2012, **31**, 938–943.
30 X. L. Wang, C. Yan, H. Hu, X. C. Zhou, R. S. Guo, X. Q. Liu, Z. Xie, Z. F. Huang and Z. J. Zheng, *Chem.–Asian J.*, 2014, **9**, 2170–2177.
31 Q. H. Gao, J. T. Hu, R. Li, Z. Xing, L. Xu, M. H. Wang, X. J. Guo and G. Z. Wu, *Radiat. Phys. Chem.*, 2016, **122**, 1–8.
32 A. A. Saraev, Z. S. Vinokurov, V. V. Kaichev, A. N. Shmakov and V. I. Bukhtiyarov, *Catal. Sci. Technol.*, 2017, **7**, 1646–1649.